Authors' Response to Reviews of

NMVOC emission optimization in China through assimilating formaldehyde retrievals from multiple satellite products

Canjie Xu[1], Jianbing Jin*[1], Ke Li[1], Yinfei Qi[2], Ji Xia[1], Hai Xiang Lin[3,4], Hong Liao[1]
Atmospheric Chemistry and Physics, 10.5194/egusphere-2025-140

RC: ***Reviewers' Comment***, AR: Authors' Response, □ Manuscript Text

1. Overview

Response to Referee 2:We would like to sincerely thank the referee for the careful review of our manuscript. We acknowledge that the original submission contained inaccuracies and shortcomings, and we are grateful that these were pointed out. We have carefully revised and corrected the manuscript in response. We truly appreciate the referee's efforts and sincerely hope that the revised version can be re-evaluated in light of these changes.

2. Major concerns

RC: ***1) The satellite data are not properly used. An important issue is filtering. Let's begin with OMI. Figure 3 shows very high columns over Tibet (2E16 molec cm-2), which are clearly impossible. This feature is not seen in other studies using OMI, e.g. Cao et al. 2018 (also using SAO OMI,) and Muller et al. 2024 (). Although OMI filtering information is missing in this manuscript, I strongly suspect that negative columns are filtered out, leading to strong positive bias in the averaged columns. The effect is most prominent in regions with low columns and high uncertainties (like Tibet), but it affects all regions. Filtering of negative values is also done by Xu et al. for TROPOMI data (see Sect. 2.3.2), which also leads to overestimation, although at a smaller extent compared to OMI, simply because TROPOMI is less noisy. Regarding OMPS, the authors claim that they "filtered out data points where the product of formaldehyde columns and three times the observation uncertainty was less than zero" (Sect. 2.3.1). This is very strange. I suppose that they meant "the sum", not the product. In any case, the filtering likely causes a positive bias.***

AR: We appreciate the reviewer's detailed diagnosis and agree that our original use of the satellite data—and, in particular, the filtering—was improper. In the initial version we (wrongly) removed negative values directly, which indeed introduces a positive bias in low-column, high-uncertainty regions (e.g., Tibet) and can yield unrealistically high averages. We also confirm the reviewer's suspicion about the typo: "product" should have been "sum"; this has been corrected.

In the revised manuscript, we have completely rewritten the description of satellite data filtering and applied clear, standardized quality control rules for all instruments. In brief, the main principles are summarized here, with the full details given in the revised manuscript:

For OMPS, we applied the recommended product screening, excluded outliers above 2×10^{17} molecules cm^{-2}, applied thresholds for solar zenith angle, cloud fraction, air mass factors, and removed negative or

unphysical values. For TROPOMI, we adopted the official QA value (>0.5) together with constraints on SZA, cloud radiance fraction, albedo, and snow/ice flags, and for OMI we followed established filtering practices considering row anomalies, cloud thresholds, and RMS fitting criteria.

After filtering, all datasets are regridded to 0.5° × 0.625° monthly means to match GEOS-Chem. Then, we tested two sampling requirements—removing grid cells with < 10 or < 50 original observations per 0.5° × 0.625° cell. Results are very similar for OMPS and TROPOMI (figures provided in the main text and Supplement), confirming low sensitivity to this choice in our focus regions. For OMI, coverage becomes sparse under these thresholds; we therefore do not use OMI as a high-resolution assimilation constraint.

With these corrections, the spurious high columns over Tibet disappear, and cross-satellite consistency improves. We re-ran all inversions, now performing two independent experiments (OMPS-only and TROPOMI-only) and removed any "combined average" design. The revised analysis (shown for 2020, with 2019 in the Supplement) includes a pre-assimilation comparison, explicit observation-uncertainty figures (vertical in the main text; spatial in the Supplement), and independent evaluation using surface ozone. In high-consistency regions/seasons, posterior ozone shows reduced biases in 81.2% of cases, with an average RMSE reduction of 24.7%.

We sincerely apologize for the earlier oversight in quality control and thank the reviewer again for pointing this out. We hope that the revised, standardized filtering and reanalysis will allow the study to be considered again with a fresh evaluation.

Text in manuscript

2.3.1 NOAA-20 OMPS

...

In this study, the quality control scheme recommended in OMPS product documentation was applied~~when using OMPS data~~. Data points with formaldehyde column densities exceeding 2e17 molecules/cm^2 were excluded to minimize the impact of outliers. After removing outliers, we further excluded data points where the sum of formaldehyde column and twice the observation uncertainty was less than zero. Furthermore, the geometric air mass factors (AMF_G) were defined as follows:

$$AMF_G = sec(SZA) + sec(VZA) \quad (1)$$

Here, SZA represents the solar zenith angle and VZA denotes the viewing zenith angle. ~~After removing outliers, we further filtered out data points where the product of formaldehyde columns and three times the observation uncertainty was less than zero. Subsequently, data points were excluded if~~ Additional data screening was applied by excluding observations with SZA ~~exceeded~~ greater than 70°, ~~the~~ an air mass factor ~~was~~ less than 0.1, ~~the~~ a geometric air mass factor ~~exceeded 5, or the cloud fraction surpassed~~ greater than 4, a cloud fraction exceeding 0.4~~. Snapshots of filtered~~ , or with positive snow and ice fractions. All screened data were then averaged to a spatial resolution of 0.5° latitude × 0.625° longitude on a monthly basis, consistent with the GEOS-Chem model configuration. To make a fair comparison between the observed and simulation formaldehyde column concentration in the assimilation, we further imposed constraints on the number of observations within each grid cell. Specifically, two filtering schemes were tested, in which grid cells with fewer than 10 or fewer

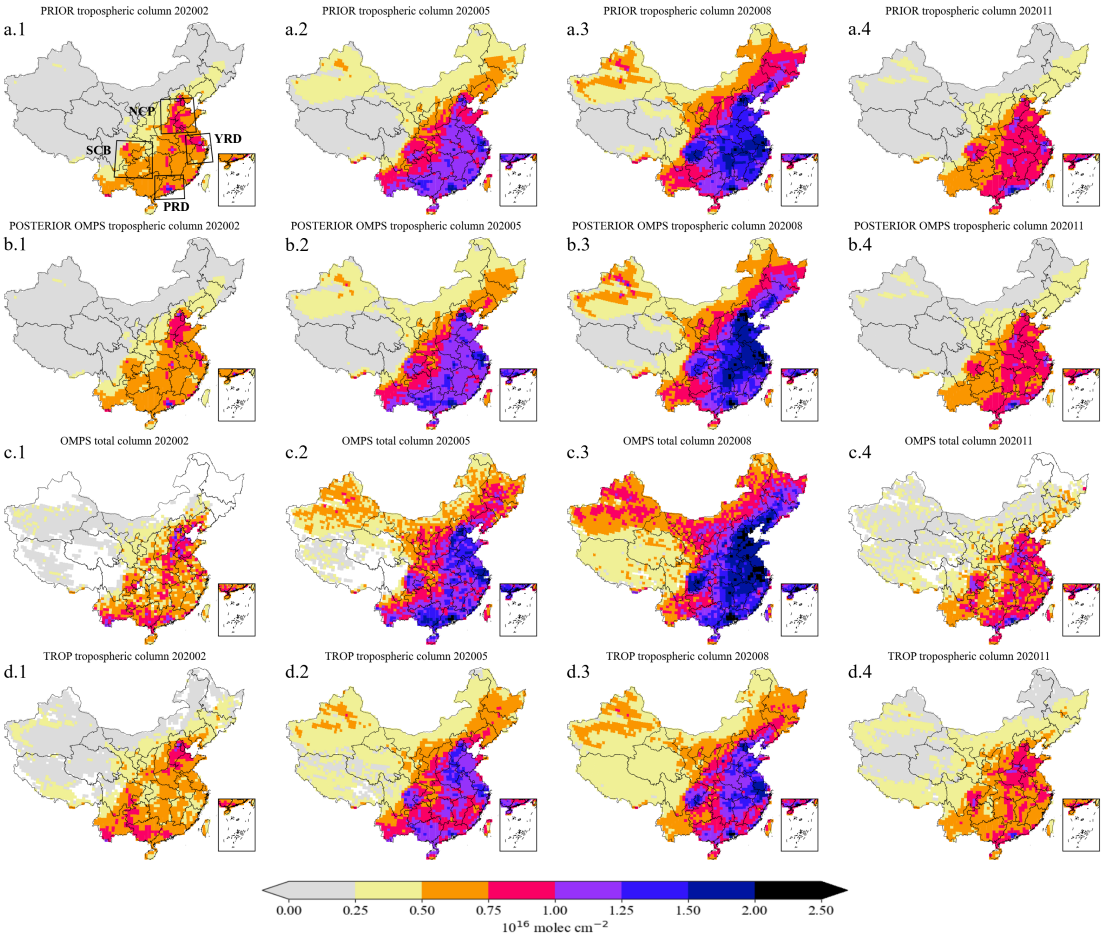

Figure 1. Spatial distributions of formaldehyde columns from GEOS-Chem model-simulated prior tropospheric columns (a) and posterior tropospheric columns constrained by OMPS assimilation (b), satellite observations of OMPS total columns (c), and satellite observations of TROPOMI tropospheric columns (d) in February (a.1-d.1), May (a.2-d.2), August (a.3-d.3), and November (a.4-d.4) of 2020.

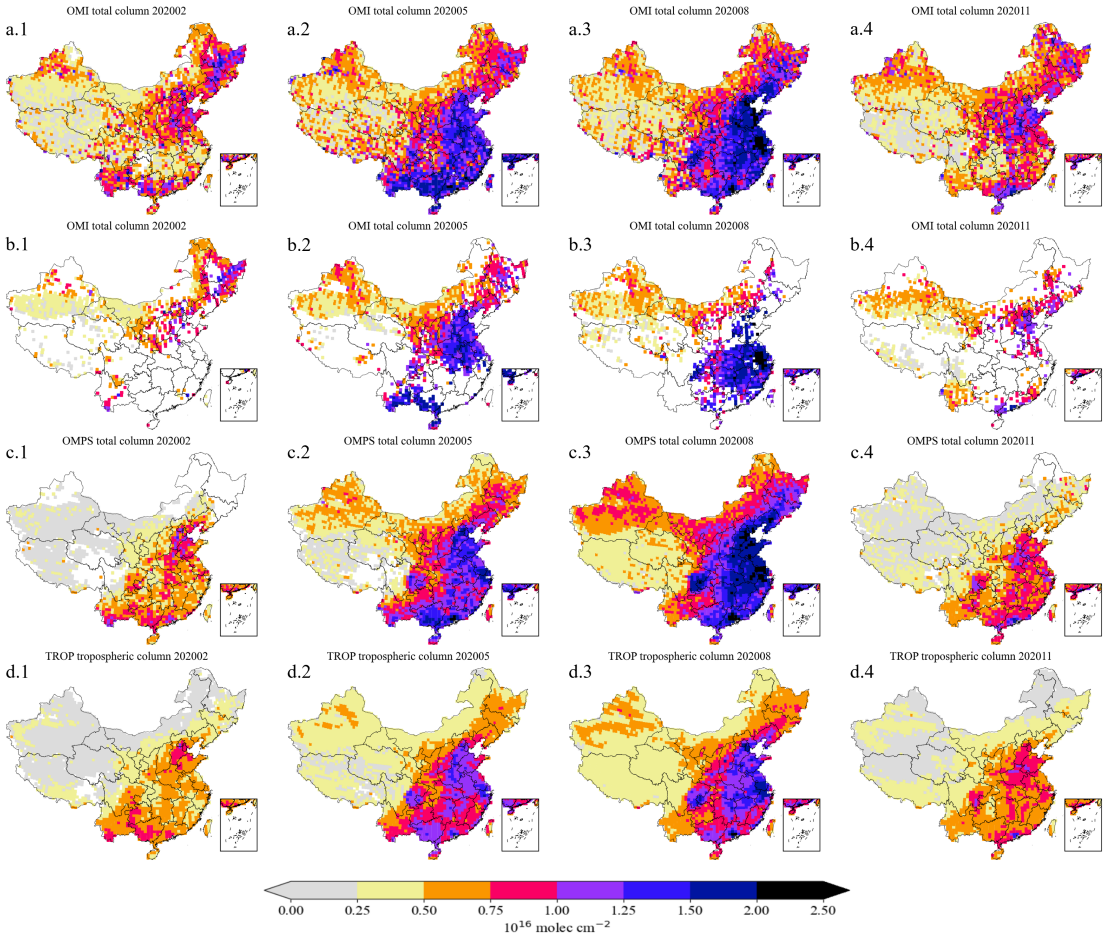

Figure 2. Comparison of monthly mean formaldehyde column concentrations in February, May, August, and November 2020 after applying different data filtering thresholds. Panels (a.1-a.4), (c.1-c.4), and (d.1-d.4) show OMI, OMPS, and TROPOMI results, respectively, after removing grid cells with fewer than 10 observations. Panels (b.1-b.4) show OMI results after removing grid cells with fewer than 50 observations.

than 50 original observations were excluded. The OMPS formaldehyde columns ~~is~~ after applying the threshold of 50 are shown in Figure ~~1(c~~1 (c), while the results with the threshold of 10 are provided in the Supplement. The differences between the two filtering schemes are minor, particularly across the four study regions considered in this work.

...

2.3.2 Sentinel-5P TROPOMI

...

When using Level 2 TROPOMI formaldehyde data for the validation in this ~~paper, we excluded only negative values and excessively large outliers to ensure data coverage. Examples of filtered TROPOMI formaldehyde columns are shown in Figure 1(d)~~study, we applied the recommended quality assurance filtering by retaining only pixels with a qa value greater than 0.5. This criterion ensures the exclusion of error flags and requires that the cloud radiance fraction at 340 nm is below 0.5, the solar zenith angle (SZA) does not exceed 70°, the surface albedo is below 0.2, no snow or ice warning is present, and the air mass factor (AMF) is larger than 0.1. The TROPOMI product provides vertical information on 34 layers, but the retrieval is primarily sensitive to the troposphere and thus reports the formaldehyde tropospheric column. After filtering, the TROPOMI observations were aggregated to monthly means on a 0.5° × 0.625° grid, ensuring consistency with the resolution used in the GEOS-Chem simulations. In addition, we further constrained the number of observations per grid cell: Figure 1 (d) shows the results after excluding grid cells with fewer than 50 observations, while the results with a threshold of 10 are also provided in the Supplement. The differences between the two filtering schemes are minor, particularly over the study regions.

...

2.3.3 Aura OMI

...

In this study, we use the OMI/Aura formaldehyde Total Column Daily L2 Global Version 3 product (Chance, 2014)~~is also used for the observation sources in this paper. The retrieval algorithm for this product is based on a nonlinear least-squares fitting technique, which calculates the slant column density (SCD) . The SCD is then converted to vertical column density (VCD) using air mass factors (AMF). Since atmospheric formaldehyde is primarily concentrated in the troposphere, the total VCD can be regarded as the tropospheric VCD of formaldehyde (Duncan et al., 2010). In practical applications, data with a cloud fraction greater than or equal to~~ . In order to minimize the influence of poor-quality data, we applied strict quality filtering. Only pixels with cloud fraction $\leqslant$ 0.3~~are further excluded~~, solar zenith angle $\leqslant$ 70°, and a main data quality flag = 0 were retained. To avoid poor-quality measurements at large pixel sizes, the five marginal pixels on each side of the swath were discarded, and only pixels within rows 6-55 were used (Zhu et al., 2017; Xue et al., 2020) . Because OMI has experienced a row anomaly since 2007, pixels with Xtrack quality flags = 0 were further selected to eliminate its impact. Additionally, given the large uncertainties in formaldehyde retrievals, pixels with a fitting root mean square (RMS) $\leqslant$ 0.003 were retained to remove most outliers (Souri et al., 2017).

The OMI observations are then aggregated to monthly means on a 0.5° × 0.625° grid, consistent with the GEOS-Chem model resolution. To ensure sufficient sampling per grid cell, we also applied two

filtering schemes based on the number of observations, excluding grid cells with fewer than 10 or fewer than 50 valid pixels. Unlike OMPS and TROPOMI, however, OMI shows a strong reduction in data coverage under these constraints, and the product becomes sparse after applying the threshold of 50 observations. This indicates that OMI suffers from insufficient sampling density in China for high-resolution assimilation. The vertical profile correction of OMI formaldehyde was conducted using the same approach as applied to OMPS, by recalculating AMF with model-simulated vertical profiles.

RC: ***2) The optimization of emissions relies on the comparison of monthly averaged modelled and satellite columns. However, the satellite average excludes cloudy pixels, whereas the model average does not. Including the cloudy days in the model averages causes a negative bias with respect to the satellite averages. Furthermore, it is not even stated whether the model columns are sampled at the satellite overpass time. This should be clarified. Finally, the manuscript makes no mention of averaging kernels (or scattering weights). Applying averaging kernels to the model profiles is essential to minimize the effect of vertical profile shapes between your model and the profiles adopted in the satellite retrieval.***

AR: We appreciate the reviewer for these valuable suggestions, which helps a lot to improve the quality of the emission inversion.

Regarding cloudy conditions, we acknowledge that cloudy pixels were not excluded from the model averages. To minimize the potential bias, we required at least 50 valid satellite pixels in each 0.5° ×0.625° grid cell when computing the monthly mean, ensuring sufficient data density and reducing the impact of outliers. The model columns were sampled between 12:00 and 14:00 local time to match the afternoon overpass of the satellites over China. Finally, we agree that applying vertical profile corrections is essential to minimize inconsistencies between model and retrieval profile shapes.

In the revised manuscript, we have substantially expanded this description. Specifically, for OMI and OMPS total column products, we recalculated air mass factors (AMF) using the model vertical profiles, while for the TROPOMI tropospheric column product, we applied the averaging kernel (AVK) method recently used in IASI v4 retrievals. These corrections increase the consistency between model simulations and satellite observations and improve the robustness of the assimilation results. Since there are too many revisions, we only list some of the key changes in this revised manuscript below. In the assimilation, OMPS retrievals are used as total columns as provided by the product, while TROPOMI retrievals are assimilated as tropospheric columns. We did not construct total columns from TROPOMI, since doing so would introduce additional uncertainties. This choice does not affect comparability, because the model provides full vertical concentration profiles that can be integrated to both total and tropospheric columns, and formaldehyde is primarily distributed below the tropopause.

Text in manuscript

2.1 Model simulation

...

Since the satellite overpasses China mainly between 12:00 and 14:00 local time, the model outputs within this time window are sampled to calculate the formaldehyde columns for fair comparison with the satellite observations. Our GEOS-Chem model outputs both total and tropospheric formaldehyde column concentrations, enabling comparison with OMPS total column data and TROPOMI formaldehyde column measurements as will be introduced later. Samples of the formaldehyde tropospheric column

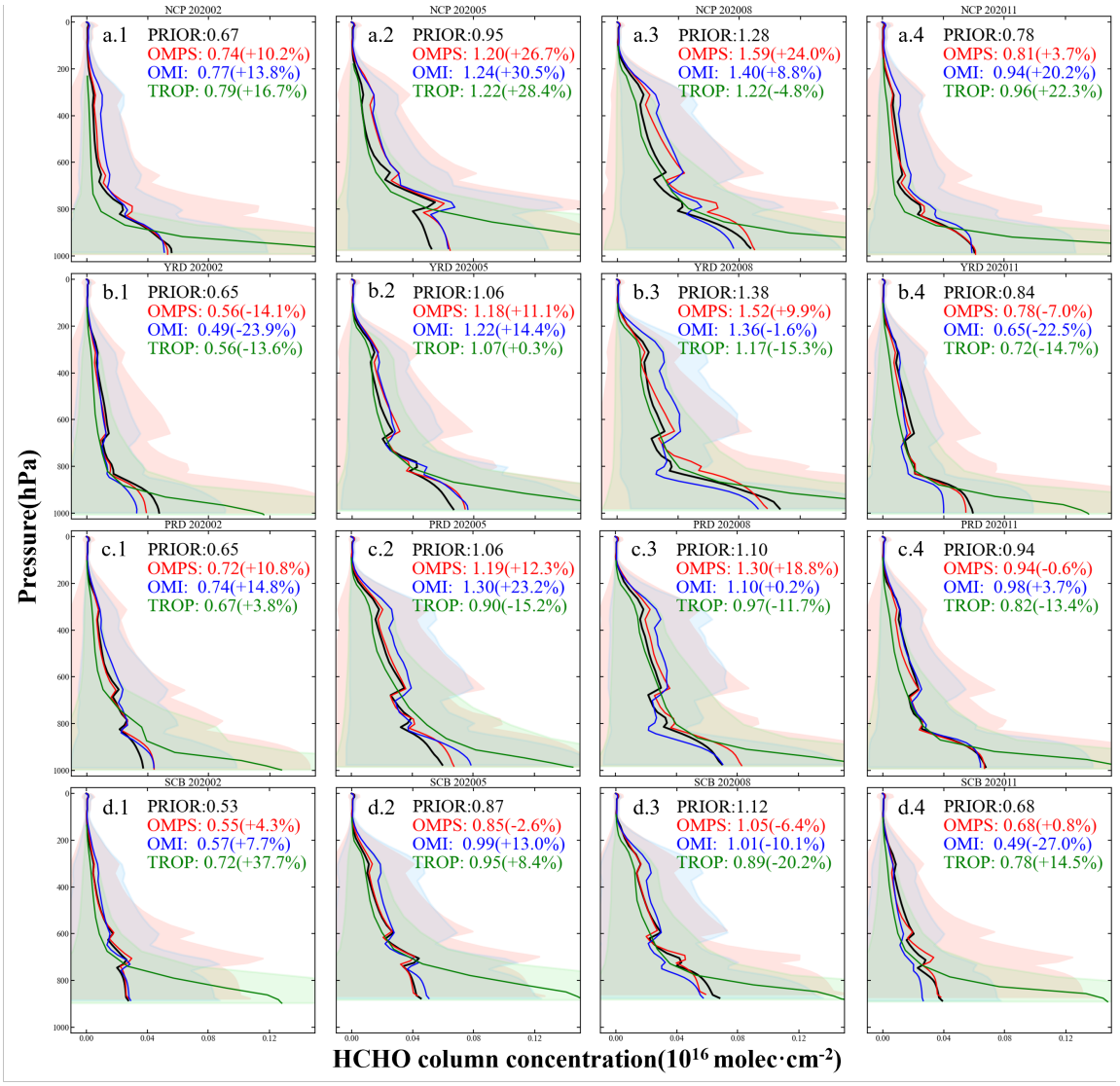

Figure 3. Vertical distributions of the regional mean formaldehyde columns from GEOS-Chem model-simulated prior (black) and satellite observations by OMPS (blue), TROPOMI (red), and OMI (green). Panels (a)-(d) correspond to the North China Plain, Yangtze River Delta, Pearl River Delta, and Northeast China, respectively. Sub-panels (a.1-d.1), (a.2-d.2), (a.3-d.3), and (a.4-d.4) represent February, May, August, and November 2020, respectively. Values in parentheses indicate the biases of satellite observations relative to the prior simulation. Shaded areas denote the observational uncertainties.

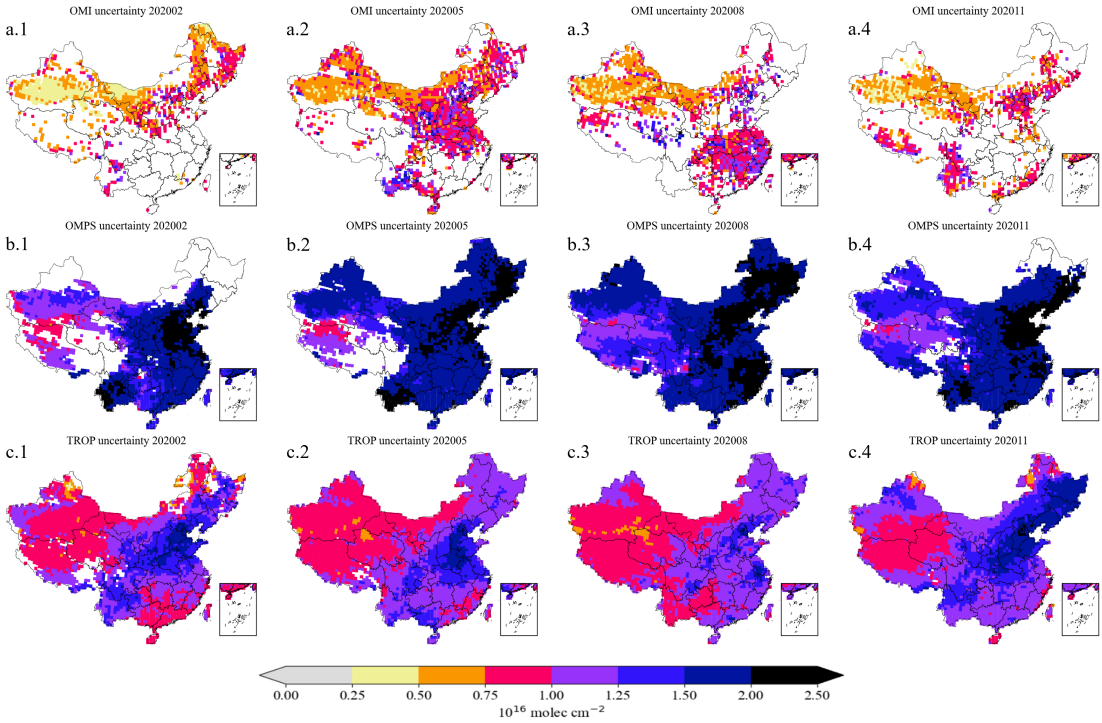

Figure 4. Uncertainties of formaldehyde column retrievals from OMI (a.1-a.4), OMPS (b.1-b.4), and TROPOMI (c.1-c.4) in February, May, August, and November 2020.

simulation are presented in Figure 1 (a).

...

2.3.1 NOAA-20 OMPS

...

To make a fair comparison between the observed and simulation formaldehyde column concentration in the assimilation, we further imposed constraints on the number of observations within each grid cell. Specifically, two filtering schemes were tested, in which grid cells with fewer than 10 or fewer than 50 original observations were excluded. The OMPS formaldehyde columns ~~is~~ after applying the threshold of 50 are shown in Figure ~~1(c~~1 (c), while the results with the threshold of 10 are provided in the Supplement. The differences between the two filtering schemes are minor, particularly across the four study regions considered in this work.

Formaldehyde vertical column densities (VCDs) retrieved from satellite observations are derived using air mass factors (AMF), which strongly depend on the a priori vertical profiles of formaldehyde. Direct comparisons between satellite products and model simulations may be biased if the a priori profiles used in the retrieval differ from the simulated ones. To ensure consistency between the satellite observations and GEOS-Chem simulation, we applied an AMF correction by recalculating the AMF with model-simulated profiles following the method used in Palmer et al. (2001):

$$AMF = \int_{p_s}^{0} w\,(p) S\,(p)\,dp \tag{2}$$

The right-hand side of the equation represents the vertically integrated product of the scattering weight $w(p)$ and the shape factor $S(p)$ as a function of pressure p, where $w(p)$ characterizes the sensitivity of the satellite measurement to a given atmospheric layer and $S(p)$ describes the normalized vertical distribution of formaldehyde. The scattering weights $w(p)$ are primarily determined by satellite observational geometry (e.g., solar and viewing zenith angles), surface albedo, and cloud fraction, while the shape factor $S(p)$ depends on the vertical profiles of formaldehyde. The integration is performed over the pressure coordinate from the surface (p_s) to the top of the atmosphere. Figure 3 illustrates the vertical distribution of the shape profile, highlighting the relative contributions of different layers. The vertical column density (VCD) is obtained from the ratio of the slant column density (SCD) to the AMF:

$$VCD = \frac{SCD}{AMF} \tag{3}$$

In the OMPS formaldehyde product, the SCD is derived as the sum of three components: the fitted differential slant column amount (ΔSCD), the reference sector correction (SCD_{Ref}), and the bias

correction (SCD_B):

$$SCD = \Delta SCD + SCD_{Ref} + SCD_B \tag{4}$$

Here, ΔSCD represents the differential slant column amount retrieved from the DOAS spectral fitting, SCD_{Ref} is the reference sector correction that accounts for background contributions and instrumental offsets by using clean reference regions, and SCD_B denotes an additional bias correction to mitigate systematic errors.

The processed OMPS satellite observations were ultimately assimilated as total columns, which are presented in Figure 1 (c.1-c.4).

...

2.3.2 Sentinel-5P TROPOMI

...

After filtering, the TROPOMI observations were aggregated to monthly means on a $0.5° \times 0.625°$ grid, ensuring consistency with the resolution used in the GEOS-Chem simulations. In addition, we further constrained the number of observations per grid cell: Figure 1 (d) shows the results after excluding grid cells with fewer than 50 observations, while the results with a threshold of 10 are also provided in the Supplement. The differences between the two filtering schemes are minor, particularly over the study regions.

Beyond the recommended quality screening, a key consideration when comparing TROPOMI formaldehyde retrievals with model outputs is the dependence on the assumed a priori vertical profile. Traditionally, studies have relied on AMF-based corrections, in which AMF is recalculated using model-derived profiles to reduce such discrepancies (Palmer et al., 2001; Boersma et al., 2004; Zhu et al., 2016; Cooper et al., 2020) . More recently, the availability of averaging kernel (AVK) information in the TROPOMI product has allowed a more consistent comparison by accounting for the impact of the assumed vertical profile shape in the retrieval, following the approach introduced in the IASI NH_3 version 4 product (Clarisse et al., 2023; Xia et al., 2025). In this study, we apply AVK-based correction for TROPOMI formaldehyde by projecting the model profiles onto the satellite pressure grid, thereby achieving a more harmonized comparison with GEOS-Chem simulations. The corrected column is calculated as:

$$\hat{X}^m = \frac{\hat{X}^a - B}{\sum_p A_p^a m_p} + B \tag{5}$$

where $\hat{X}^m$ denotes the formaldehyde column adjusted with the model profile, $\hat{X}^a$ is the retrieved column based on the a priori profile, and B is the background concentration. The term A_p^a represents the AVK at pressure level p, and m_p is the normalized model shape factor at the same level, defined

as:

$$m_p = \frac{M_p^m - B_p}{M^m - B} \tag{6}$$

The processed TROPOMI retrievals were assimilated as tropospheric columns, which are presented in Figure 1 (d.1-d.4), with their vertical shape profiles shown in Figure 3 (green line) to illustrate the normalized contribution of each pressure layer to the tropospheric columns. We adopted tropospheric rather than total columns because the retrieval product itself provides tropospheric columns, and recalculating total columns would introduce substantial uncertainties.

2.3.3 Aura OMI

...

The OMI observations are then aggregated to monthly means on a $0.5° \times 0.625°$ grid, consistent with the GEOS-Chem model resolution. To ensure sufficient sampling per grid cell, we also applied two filtering schemes based on the number of observations, excluding grid cells with fewer than 10 or fewer than 50 valid pixels. Unlike OMPS and TROPOMI, however, OMI shows a strong reduction in data coverage under these constraints, and the product becomes sparse after applying the threshold of 50 observations. This indicates that OMI suffers from insufficient sampling density in China for high-resolution assimilation. The vertical profile correction of OMI formaldehyde was conducted using the same approach as applied to OMPS, by recalculating AMF with model-simulated vertical profiles.

...

3.1 Satellite data evaluation

...

DIFaddbegin Uncertainty is a key component in the assimilation process and serves as a crucial indicator of satellite data quality. Figure 3 illustrates the vertical distribution of retrieval uncertainties. In the mid- to upper troposphere (200-600 hPa), OMPS and OMI show comparable levels of uncertainty. However, below 600 hPa, OMPS uncertainties become substantially larger, likely due to cloud contamination and retrieval algorithm approximations (González Abad et al., 2016; Nowlan et al., 2023). As shown in ~~the four interpolated results in Figure 3, the spatial distribution of high formaldehyde values is consistently captured across different horizontal resolutions, either by the satellite observations in Figure 3~~Supplementary Figure S2, the overall uncertainty of OMPS is significantly higher than that of the other two satellite datasets. At first glance, OMI data may appear superior, but this advantage largely results from strict filtering, which excludes a substantial fraction of problematic data. As illustrated in Supplementary Figure S3 (a, b~~, c)or by GEOS-Chem simulation in panel (d). These hot spots are particularly prominent in the North China Plain (NCP) and Jiangsu-Zhejiang-Shanghai regions. However, at the higher resolution of 0.5° × 0.5°, OMI formaldehyde data exhibits noticeable noise all over China and lacks the spatial continuity observed in TROPOMI, OMPS, and GEOS-Chem datasets. The significant spatial variability in the NMVOC emission field might account for the discontinuity observed in OMI formaldehyde data . However, this discontinuity contradicts the model~~

simulation and the other two satellite products obtained from the more advanced instruments. Moreover, such discontinuities are not observedin OMI formaldehyde retrievals over the United States, where (Kaiser et al., 2018) demonstrated continuous and high-quality data. Therefore, the discrepancies observed in China may be attributed to uncertain input parameters, such as aerosols and surface albedo. OMI formaldehyde retrievals with larger spatial grid intervals (2° × 2°), applying a threshold of 50 observations per grid cell drastically reduces spatial coverage, rendering OMI unsuitable for national-scale assimilation. Previous studies that assimilated OMI over China have typically interpolated the data to coarser resolutions to ensure applicability (Cao et al., 2018; Miyazaki et al., 2020). Therefore, only OMPS and 4° × 4°) exhibit increased continuity and smoothness, as shown in Figure 3(a). This improvement is attributed to spatial averaging, which effectively filters out white noise (Lee, 1980).

The differences in spatial variability among OMI, OMPS, TROPOMI, and GEOS-Chem simulations are clearly illustrated in the semi-variogram plot shown in Figure 4. In this plot, smaller semi-variance values indicate stronger spatial autocorrelation and smaller random noise. We define the area below the yellow line in Figure 4 as the "stable zone" of the semi-variance plot, which represents regions where the data effectively capture the true spatial dynamics of atmospheric formaldehyde. The semi-variance plots demonstrate that the semi-variance function curves of GEOS-Chem, TROPOMI, and OMPS formaldehyde column data consistently fall within the stable zone across all spatial grids. In contrast, the semi-variance function curve of OMI formaldehyde data only enters the stable zone at coarser spatial resolutions of 2° × 2° or even 4° × 4°. This observation suggests that at these coarser spatial resolutions, OMI formaldehyde data for China achieves sufficient continuity and reliability. This finding is consistent with study in Cao et al. (2018), which constrained NMVOC emissions in China at a coarse resolution of 4° × 5°. TROPOMI formaldehyde columns are assimilated in this study, while OMI is excluded for our high-resolution emission inversion due to the poor data coverage.

Figure 3 also presents satellite retrieval deviations from the prior model estimates. When all three satellite datasets exhibit the same sign of deviation (positive or negative) relative to the model, they are considered consistent. Such consistency is observed, for example, in February, May, and November over NCP and in February over PRD and SCB, where all three datasets show positive deviations; and in February and November over YRD and in August over SCB, where all show negative deviations. These cases indicate stronger reliability. In other situations, when OMPS and TROPOMI exhibit the same bias direction, they are also considered consistent, as in November over PRD and SCB. Overall, at higher spatial resolutions, OMI formaldehyde data exhibit more white noise, with higher semi-variance values and weaker spatial autocorrelation. In contrast, the semi-variance values of OMPS and TROPOMI align more closely with the trends observed in GEOS-Chem, making them more suitable for high-resolution (<1°) emission optimization. 10 out of 16 cases (62.5%) exhibit consistency, with higher coherence primarily occurring in the cold season and during spring and autumn months over NCP and SCB. Subsequent analyses will explicitly consider this consistency to enhance the robustness of the conclusions.

...

3.3 Formaldehyde columns evaluation

...

The spatial distributions of formaldehyde columns in February, May, August, and November 2020 are shown in Figure 1 (a) and (b), GEOS-Chem simulated the prior and posterior estimates of formaldehyde for four months of the year 2020 over China. In Figure 1 (a) , the prior results exhibit a spatial

~~distribution similar to satellite observations . When compared to OMPS and~~ 1. Panels (a.1-a.4) display the prior simulations of tropospheric columns, (b.1-b.4) present the posterior simulations of tropospheric columns assimilated by OMPS, (c.1-c.4) show the OMPS satellite observations of total columns, and (d.1-d.4) illustrate the TROPOMI satellite observations of tropospheric columns. In addition, the prior ~~results accurately reproduce high-value features in most regions, including Yunnan-Guizhou, Guangxi-Guangdong, NCP, the southeastern coast, and the northeast. However, the previous simulation did not accurately represent the actual formaldehyde levels. Specifically, it underestimated formaldehyde concentrations to varying degrees across different regions. By assimilating OMPS formaldehyde columns, improvement was obtained steadily in the posterior simulations. Nationwide, the posterior formaldehyde columns were raised by approximately 50%. Comparing to TROPOMI data used as independent measurements, the~~ and posterior simulations of total columns for 2020 are also provided in the Supplementary Figure S7. As indicated by the vertical profiles in Figure 3, formaldehyde ~~levels~~ is mainly distributed below the tropopause. Comparisons between the prior and posterior results show that the differences between total and tropospheric columns are relatively small. Regarding the spatial patterns, high formaldehyde values in February are concentrated in the NCP~~region were raised from less than 1.2 $\times 10^{16}$ molec/cm^2 to around 2.4 $\times 10^{16}$ molec/cm^2 in January, closer to the observed values either from OMPS and TROPOMI. The~~ , YRD, and PRD regions, with the posterior results showing an expanded high-value ~~features in Yunnan-Guizhou became more prominent in April, and significant improvements were also observed in the southeastern coast, NCP, and the northeast in July and October. However,~~ area in the NCP but a reduced coverage in the YRD. In May, overall concentrations increase nationwide, with particularly pronounced growth in the NCP and PRD. In August, concentrations increase in the NCP, YRD, and PRD, while they decrease in the SCB. In November, the changes are modest, but all four regions exhibit reduced concentrations.

RC: ***3) TROPOMI and OMI HCHO products have significant biases – see Zhu et al. (), Vigouroux et al. 2020 (), Oomen et al. 2024 (), Muller et al. 2024 (https://doi.org/10.5194/acp-24-2207-2024). I am not sure whether OMPS data were similarly evaluated. In any case, the biases should be either corrected for, or discussed within the manuscript, as well as the potential implications for the emissions.***

AR: We thank the reviewer for this important comment. By reviewing the literature (Zhu et al.; Vigouroux et al., 2020; Oomen et al., 2024; Müller et al., 2024) and comparing with their results, we realized that our satellite datasets indeed showed biases relative to previous studies. The treatment of these biases and their implications have already been explained in RC 1 and RC 2. In the revised manuscript, we have clarified this point and ensured that our data processing now follows approaches consistent with, or stricter than, those used in earlier work, so that the satellite inputs to our assimilation are comparable and reliable. We also apology that we did not conduct bias correction before assimilation in this study since we don't have independent surface or aircraft-based measurements.

RC: ***4) The methodology is not well described. For example:***

AR: We thank the reviewer for these detailed comments. Our replies are as follows:

RC: ***- no detail is provided on the implementation of MEGAN, besides the fact that the emissions are calculated off-line. What is their temporal resolution, what meteorological fields are used, what vegetation maps and emission factors, etc.?***

AR: In this study, MEGAN emissions were not generated by running MEGAN separately. Instead, they were provided directly through the HEMCO module of GEOS-Chem and used as an offline inventory. The data

were interpolated to 0.5° × 0.625° to match the model resolution. This point has been clarified in the revised manuscript.

Text in manuscript

2.2 Prior NMVOC emission inventories

...

Before these prior emissions are used to drive GEOS-Chem simulations, the spatial resolution is coarsened to an average value on a 0.5° ~~×~~ × 0.625° grid resolution consistent with the model configuration as used in Section 2.1.

Figure 5 (a) presents the prior NMVOC emission inventories for 2020, which primarily relies on the anthropogenic emission inventory from MEIC, supplemented by the CEDS inventory for species not included in MEIC. Additionally, ~~the biogenic emission inventory from~~ biogenic emissions are provided by MEGAN (offline calculation) ~~and the biomass burning inventory~~ for the year 2020 with an hourly temporal resolution, directly through the HEMCO emission component of GEOS-Chem; in this study, we did not run the MEGAN model separately. Biomass burning emissions are taken from GFED4~~are incorporated. The optimization of NMVOC emissions through the assimilation of formaldehyde observations will be conducted using these combined prior inventories.~~ . The combination of these three sources is treated as the prior emission inventory used in the following NMVOC emission optimization.

RC: ***- the description of OMI data is too short***

AR: We have expanded the description of the OMI HCHO dataset in the revised manuscript.

Text in manuscript

2.3.3 Aura OMI

The Ozone Monitoring Instrument (OMI) is an important satellite instrument ~~mounted on~~ onboard the Aura satellite, launched on July 15, ~~2004. Its purpose is to monitor and study the composition of~~ 2004, with the objective of monitoring atmospheric gases, aerosols, and clouds to ~~enhance~~ improve our understanding of atmospheric chemistry and climate change. OMI provides daily global coverage with ~~high spatial resolution (~~a wide swath of 2600 km and a spatial resolution of approximately 13 ~~×~~ × 24 km ~~), and its wide swath (2600 km) allows it to achieve global coverage in one day. It overpasses at~~ at nadir, with an equator crossing time of about 13:45 LT~~each day. OMI~~ . The sensor contains three spectral channels ~~: (~~UV-1, UV-2, and VIS), covering the wavelength ranges of ~~264–311 nm, 307–383~~ 264-311 nm, 307-383 nm, and ~~349–504~~ 349-504 nm, respectively~~. These channels enable the observation of various trace gases , ~~, which enable the retrieval of key trace gases including O_3, ~~nitrogen dioxide (~~NO_2~~), sulfur dioxide (~~, SO_2~~)~~, and formaldehyde (Zhang et al., 2019).

In this study, we use the OMI/Aura formaldehyde Total Column Daily L2 Global Version 3 product (Chance, 2014)~~is also used for the observation sources in this paper. The retrieval algorithm for this product is based on a nonlinear least-squares fitting technique, which calculates the slant column density (SCD) . The SCD is then converted to vertical column density (VCD) using air mass factors (AMF). Since atmospheric formaldehyde is primarily concentrated in the troposphere, the total VCD can be regarded as the tropospheric VCD of formaldehyde (Duncan et al., 2010). In~~

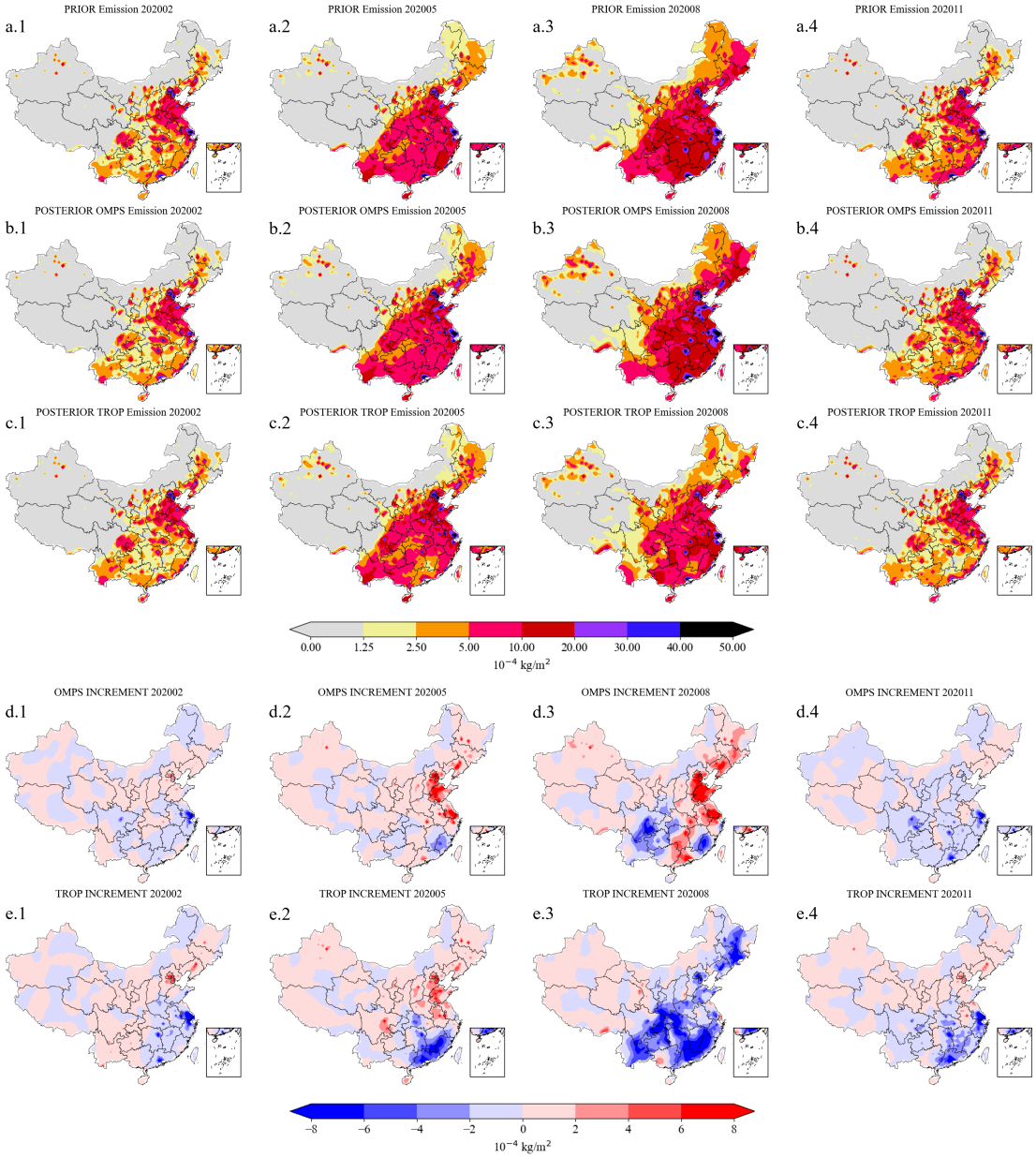

Figure 5. Spatial distributions of the total NMVOC emissions from the prior (a) and posterior (b) results in ~~January~~ February (a.1, b.1), ~~April~~ May (a.2, b.2), ~~July~~ August (a.3, b.3), ~~October~~ November (a.4, b.4) 2020. Panels (d.1-d.4) and (e.1-e.4) show the corresponding emission increments (posterior minus prior) derived from OMPS and TROPOMI assimilation.

~~practical applications, data with a cloud fraction greater than or equal to~~ . In order to minimize the influence of poor-quality data, we applied strict quality filtering. Only pixels with cloud fraction $\leqslant$ 0.3~~are further excluded~~, solar zenith angle $\leqslant$ 70°, and a main data quality flag = 0 were retained. To avoid poor-quality measurements at large pixel sizes, the five marginal pixels on each side of the swath were discarded, and only pixels within rows 6-55 were used (Zhu et al., 2017; Xue et al., 2020) . Because OMI has experienced a row anomaly since 2007, pixels with Xtrack quality flags = 0 were further selected to eliminate its impact. Additionally, given the large uncertainties in formaldehyde retrievals, pixels with a fitting root mean square (RMS) $\leqslant$ 0.003 were retained to remove most outliers (Souri et al., 2017).

The OMI observations are then aggregated to monthly means on a 0.5° $\times$ 0.625° grid, consistent with the GEOS-Chem model resolution. To ensure sufficient sampling per grid cell, we also applied two filtering schemes based on the number of observations, excluding grid cells with fewer than 10 or fewer than 50 valid pixels. Unlike OMPS and TROPOMI, however, OMI shows a strong reduction in data coverage under these constraints, and the product becomes sparse after applying the threshold of 50 observations. This indicates that OMI suffers from insufficient sampling density in China for high-resolution assimilation. The vertical profile correction of OMI formaldehyde was conducted using the same approach as applied to OMPS, by recalculating AMF with model-simulated vertical profiles.

RC: ***- the motivation and added value of the semi-variogram analysis is not clear. No surprise that OMI data are revealed to be more noisy than the other datasets, since year 2020 is used here, >15 years after the launch of OMI.***

AR: We agree with the reviewer that the original treatment was inappropriate. After reprocessing and re-evaluation, we have decided to follow the reviewer's advice and remove the semi-variogram analysis from the manuscript.

RC: ***- more information is needed to explain the details of how emissions are really optimized. The assumed uncertainty on the prior emissions should be given and justified.***

AR: We thank the reviewer for this important comment. Following Souri et al. (2020), we assigned sector-specific prior uncertainties of 150% for anthropogenic VOCs, 200% for biogenic VOCs, and 300% for biomass burning VOCs. These uncertainties were combined using a weighted quadratic formulation, which yielded an overall uncertainty of about 120%; accordingly, the standard deviation of the multiplicative factor was set to 0.4. This treatment is now explicitly described in the manuscript with supporting references. We have also clarified that the optimization is performed using a 4DEnVar data assimilation system, which is adjoint-free and based on ensemble linearization of the GEOS-Chem formaldehyde simulation. Additional details concerning the algorithm, regularization, convergence, and assimilation setup have been added in the revised manuscript and the Supplement.

Text in manuscript

Table 1. Uncertainty assumptions for different emission sectors.

	Anthropogenic	Biogenic	Biomass burning
VOC	150%	200%	300%

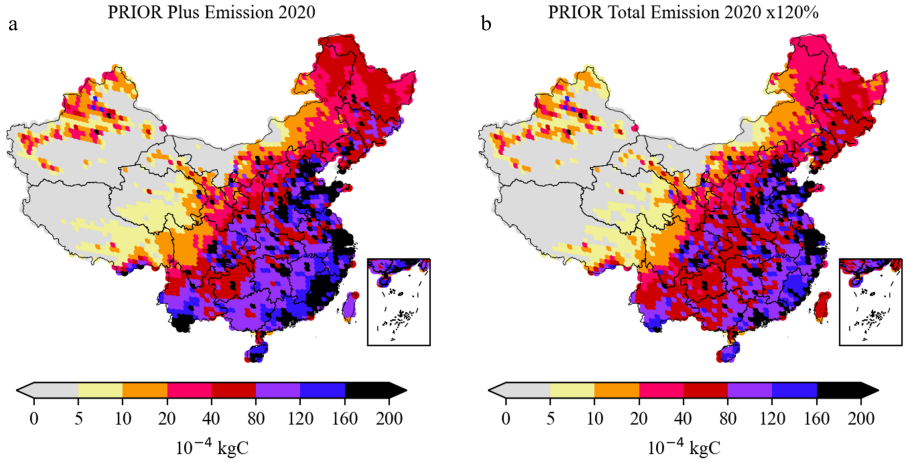

Figure 6. Comparison of prior NMVOC emissions estimated by combining sector-specific uncertainties (a) and by uniformly scaling the prior total emissions by 120% (b) in 2020. The two distributions are generally consistent, supporting the applicability of the total uncertainty assumption used in this study.

2.5 Assimilation algorithm

This study employs the four-dimensional ensemble variational (4DEnVar) methodology to ~~assimilate formaldehyde observations to constrain NMVOC emissions~~ optimize NMVOC emissions with satellite formaldehyde observations. The goal of ~~this~~ the assimilation is to find the most likely estimate of the state vector, which is the monthly NMVOC emission inventories $\boldsymbol{f}$ over the entire model domain. Note that $\boldsymbol{f}$ represents the vector of total NMVOC emissions, rather than separately gridded anthropogenic, biogenic, or biomass burning VOC emissions. To optimize emissions from these three sectors, additional observations or a well-defined spatial correlation structure are required, which are not available in this study. The prior estimate $\boldsymbol{f}_b$ is from the inventories described in Section 2.2, and the formaldehyde concentration observations $\boldsymbol{y}$ are described in Section 2.3. Mathematically, assimilation is performed via minimizing the cost function J as follows:

$$\mathcal{J}(\boldsymbol{f}) = \frac{1}{2}(\boldsymbol{f}-\boldsymbol{f}_b)^T\mathbf{B}^{-1}(\boldsymbol{f}-\boldsymbol{f}_b) + \frac{1}{2}\{\boldsymbol{y}-\mathcal{HM}(\boldsymbol{f})\}^T\mathbf{O}^{-1}\{\boldsymbol{y}-\mathcal{HM}(\boldsymbol{f})\} \quad (7)$$

The cost function $\mathcal{J}$ is the sum of two ~~part~~parts: background and observation penal term. The background term quantifies the difference between the optimal $\vec{f}$ and the prior emission inventories $\vec{f}_b$, while the observation term calculates the difference between the simulation driven by $\vec{f}$ and the satellite observations $\vec{y}$. In addition to the $\boldsymbol{f}_b$ that represents the prior NMVOC emission vector calculated from the anthropogenic, biogenic, and biomass burning sources as been illustrated in Section 2.2. The uncertainty in the NMVOCs simulation is assumed to be attributed to errors in the emission inventories,

and can be compensated using a spatially varying tuning factor α:

$$f(i) = f_b(i) \cdot \alpha(i) \tag{8}$$

in here $f_b(i)$ denotes the NMVOC emission rate in the given grid cell i. The α values are defined to be random variables with a mean of 1.0, a minimum of 0.1 and a standard deviation ~~$\sigma_\alpha = 0.2$~~of 0.4, corresponding to a uniform 120% uncertainty applied to the total NMVOC emissions rather than sector-specific settings as adopted in previous studies (Choi et al., 2022; Jung et al., 2022; Souri et al., 2020) . The rationale for this choice is provided in the Supplement. This empirical value was found to provide sufficient spaces for resolving the observation-minus-simulation errors. A background covariance $\mathbf{B}_\alpha$ is formulated as a product of the constant standard deviation and a spatial correlation matrix $\mathbf{C}$:

$$\mathbf{B}_\alpha(i,j) = \sigma_\alpha \cdot \mathbf{C}(i,j) \tag{9}$$

where $\mathbf{C}(i,j)$ represents a distance-based spatial correlation between two αs in the grid cell i and j, and is defined as:

$$\mathbf{C}(i,j) = e^{-(d_{i,j}/l)^2/2} \tag{10}$$

where $d_{i,j}$ represents the distance between two grid cells i and j. l here denotes the correlation length scale which controls the spatially variability freedom of the αs. A small value of l ~~means more errors in fine scale could be resolved using the assimilation, while however requires more~~ indicates that the tuning factors αs are less spatially correlated, thereby enabling emission optimization at a finer spatial scale. However, this also necessitates a larger number of ensemble runs to adequately represent the model realization from emission to simulation. An empirical ~~parameterl~~ parameter l = 300 km which is used in Jin et al. (2023) to nudge the ammonia emission that has a rapid spatially variability is also taken in this study. With the covariance matrix $\mathbf{B}_\alpha$, the NMVOC emission background covariance $\mathbf{B}$ is obtained via a Schur Product:

$$\mathbf{B} = \mathbf{B}_\alpha \circ \mathbf{C} \tag{11}$$

In the observation term, $\boldsymbol{y}$ is the observation vector, representing satellite observations, $\mathcal{M}$ is the GEOS-Chem model driven by emissions $\boldsymbol{f}$, $\mathcal{H}$ is the observation operator that ~~transfer the three dimensional~~ transfers the three-dimensional concentration into the observational space, and $\mathbf{O}$ is the observation covariance matrix. In this study, the assimilated observations include the OMPS total columns and TROPOMI tropospheric columns. A distinct observation operator $\mathcal{H}$ is configured to enable a fair comparison of the observation-minus-simulation mismatch. The satellite formaldehyde observations are assumed to be independent, therefore $\mathbf{O}$ is a diagonal matrix. The diagonal value here is calculated

as:

$$\sigma_{\text{total}} = \sqrt{\sigma^2_{\text{instrument}} + \sigma^2_{\text{represent}}} \tag{12}$$

In ~~the~~ Equation 12, σ_{total} is defined as the total uncertainty, which is the square root of the sum of the squares of the instrument uncertainty $\sigma_{\text{instrument}}$ from the formaldehyde observations and the representative uncertainty $\sigma_{\text{represent}}$ introduced when processing the data into monthly averages. The representative uncertainty $\sigma_{\text{represent}}$ is represented by the standard deviation of the data.

~~With the assimilation-based emission inversion system above, we conducted three sets of experiments to explore the benefits to emission optimization. These experiments involved assimilating OMPS data and validating the assimilation results using TROPOMI, assimilating TROPOMI data, and finally assimilating the combined OMPS and TROPOMI data by averaging them. In the subsequent results, we primarily analyze the results of the first set of experiments, while the detailed inventories of the latter two experiments are archived in~~ The spatial distribution of the total uncertainty is provided in Figure 4 in the Supplement.

The assimilation methodology used in this paper is the four-dimensional ensemble variational (4DEnVar). Different from the classic 4DVar that requires adjoint in the cost function minimization, 4DEnVar emulates the GEOS-Chem formaldehyde simulating model using an ensemble-based linear approximation and hence is adjoint-free. The method is first proposed by Liu et al. (2008) and successfully implemented in our recent dust aerosol (Jin et al., 2021) and ammonia emission inversion (Jin et al., 2023; Xia et al., 2025). The detailed procedures for minimizing the cost function Equation 7 are illustrated in section 'Minimization of the Cost Function in 4DEnVar' in supplementary material.

...

Supplement

1 Emission Uncertainty

Following previous studies (Souri et al., 2020), sector-specific prior uncertainties for anthropogenic, biogenic, and biomass burning emissions can be combined into a total uncertainty using a weighted approach.

$$\sigma^2_{\text{total}} = f^2_{\text{anthro}} \cdot \sigma^2_{\text{anthro}} + f^2_{\text{biogenic}} \cdot \sigma^2_{\text{biogenic}} + f^2_{\text{bioburn}} \cdot \sigma^2_{\text{bioburn}} \tag{13}$$

Applying this method to the uncertainty values reported in earlier work, we obtained a total prior uncertainty of 120.22%. Accordingly, we set the standard deviation of the multiplicative factor to 0.4 in this study. To assess the validity of this simplification, we compared the sector-weighted prior emissions (Figure 6 (a)) with the prior emissions uniformly scaled by 120% (Figure 6 (b)). The two results are generally consistent, supporting the reasonableness of adopting a uniform total uncertainty in this study. Sector-specific inversion will be considered in future work.

...

2 Minimization of the Cost Function in 4DEnVar

The minimization of the cost function follows the 4DEnVar processes. An ensemble of emission inventory is generated randomly using the prior emission vector f and the assumed emission error covariance $\mathbf{B}$:

$$[f_1, \ldots, f_N] \tag{14}$$

An ensemble of GEOS-Chem model simulations is then forward run with the ensemble emission inventories in parallel:

$$[\mathcal{M}(f_1), \ldots, \mathcal{M}(f_N)] \tag{15}$$

Denote the emission ensemble perturbation matrix by:

$$F' = \frac{1}{\sqrt{N-1}}[f_1 - \bar{f}, \ldots, f_N - \bar{f}] \tag{16}$$

and the mean of ensemble simulation by:

$$\mathcal{M}(\bar{f}) = \frac{1}{N}\sum_{i=1}^{N}\mathcal{M}(f_i) \tag{17}$$

where $\bar{f}$ is the mean of the ensemble emission inventories. In the 4DEnVar assimilation algorithm, the optimal emission f is defined as a weighted sum of the columns of the perturbation matrix F' using weights from a control variable vector w:

$$f = \bar{f} + F'w \tag{18}$$

The cost function could then be reformulated as:

$$\mathcal{J}(w) = \frac{1}{2}w^T w + \frac{1}{2}\left\{H\mathcal{M}'w + H\mathcal{M}(\bar{f}) - y\right\}^T \mathbf{O}^{-1}\left\{H\mathcal{M}'w + H\mathcal{M}(\bar{f}) - y\right\} \tag{19}$$

where $\mathcal{M}$ is the linearization of the GEOS-Chem formaldehyde simulating model required for cost function minimization, and is approximated by:

$$\mathcal{M}'F' \approx \frac{1}{\sqrt{N}}\left[\mathcal{M}(f_1) - \mathcal{M}(\bar{f}), \ldots, \mathcal{M}(f_N) - \mathcal{M}(\bar{f})\right] \tag{20}$$

With the uncertainty in emission transferred into the observation space, the minimum of the cost function in Equation 19 could then be directly calculated, and the posterior emission f subsequently updated.

$$m_z = \frac{M_z^m - B_z}{M^m - B} \tag{21}$$

Here M_z^m represents the modeled concentration of formaldehyde at altitude z, B_z is the background concentration of formaldehyde at the same altitude, M^m represents the total modeled concentration of formaldehyde in the atmosphere, and B is the total background concentration.

$$A_z^a = \frac{1}{N}\frac{\hat{X}^a - B}{\hat{X}^l - B} \tag{22}$$

Here X_z^a represents the a priori (or assumed) concentration of formaldehyde at altitude z, B_z is again the background concentration at the same altitude, $\hat{X}^a$ is the total a priori concentration, and N is a normalization factor ensuring the matrix A_z^a sums correctly to account for all altitudes.

RC: ***- it is impossible to understand some sentences, for example (l. 14 on page 10) "A small l means more errors in fine scale could be resolved using the assimilation, while however requires more ensemble runs to represent the model realization from emission to simulation". Please clarify.***

AR: To make it clear, "A small l means more errors in fine scale could be resolved using the assimilation, while however requires more ensemble runs to represent the model realization from emission to simulation" is now changed to "A small value of l indicates that the tuning factors αs are less spatially correlated, thereby enabling emission optimization at a finer spatial scale. However, this also necessitates a larger number of ensemble runs to adequately represent the model realization from emission to simulation."

RC: ***- the representativity error is taken as the standard deviation of the columns around their monthly means: see remark above on the temporal sampling issue. This error can and should be taken care of through appropriate sampling of model concentrations.***

AR: We agree with the reviewer's point and have redone the temporal sampling of model data to be consistent with satellite overpass times.

Text in manuscript

2.1 Model simulation

...

Since the satellite overpasses China mainly between 12:00 and 14:00 local time, the model outputs within this time window are sampled to calculate the formaldehyde columns for fair comparison with the satellite observations. Our GEOS-Chem model outputs both total and tropospheric formaldehyde column concentrations, enabling comparison with OMPS total column data and TROPOMI formaldehyde column measurements as will be introduced later. Samples of the formaldehyde tropospheric column simulation are presented in Figure 1 (a).

RC: ***- from Sect. 2.3.1, it would seem that geometric air mass factors are used for the OMPS retrieval, which is very strange since the retrieval described by Nowlan et al. 2023 () incorporates a detailed AMF calculation. This should be clarified. If really geometric AMFs are being used, the product would be inappropriate for emission optimization.***

AR: After carefully checking the product documentation, we confirm that geometric AMFs were not used in calculating VCDs. This variable only appeared during the initial data screening, while the actual AMF construction for VCDs followed the retrieval algorithm described by Nowlan et al. (2023).

Text in manuscript

2.3.1 NOAA-20 OMPS

...

In this study, the quality control scheme recommended in OMPS product documentation was applied~~when using OMPS data~~. Data points with formaldehyde column densities exceeding 2e17 molecules/cm^2 were excluded to minimize the impact of outliers. After removing outliers, we further excluded data points where the sum of formaldehyde column and twice the observation uncertainty was less than zero. Furthermore, the geometric air mass factors (AMF_G) were defined as follows:

$$AMF_G = sec(SZA) + sec(VZA) \tag{23}$$

Here, SZA represents the solar zenith angle and VZA denotes the viewing zenith angle. ~~After removing outliers, we further filtered out data points where the product of formaldehyde columns and three times the observation uncertainty was less than zero. Subsequently, data points were excluded if~~ Additional data screening was applied by excluding observations with SZA ~~exceeded~~ greater than 70°, ~~the~~ an air mass factor ~~was~~ less than 0.1, ~~the~~ a geometric air mass factor ~~exceeded 5, or the cloud fraction surpassed~~ greater than 4, a cloud fraction exceeding 0.4~~. Snapshots of filtered~~ , or with positive snow and ice fractions. All screened data were then averaged to a spatial resolution of 0.5° latitude × 0.625° longitude on a monthly basis, consistent with the GEOS-Chem model configuration. To make a fair comparison between the observed and simulation formaldehyde column concentration in the assimilation, we further imposed constraints on the number of observations within each grid cell. Specifically, two filtering schemes were tested, in which grid cells with fewer than 10 or fewer than 50 original observations were excluded. The OMPS formaldehyde columns ~~is~~ after applying the threshold of 50 are shown in Figure ~~1(c~~1 (c), while the results with the threshold of 10 are provided in

the Supplement. The differences between the two filtering schemes are minor, particularly across the four study regions considered in this work.

...

Formaldehyde vertical column densities (VCDs) retrieved from satellite observations are derived using air mass factors (AMF), which strongly depend on the a priori vertical profiles of formaldehyde. Direct comparisons between satellite products and model simulations may be biased if the a priori profiles used in the retrieval differ from the simulated ones. To ensure consistency between the satellite observations and GEOS-Chem simulation, we applied an AMF correction by recalculating the AMF with model-simulated profiles following the method used in Palmer et al. (2001):

$$AMF = \int_{p_s}^{0} w\,(p) S\,(p)\,dp \tag{24}$$

RC: ***5) The results are insufficiently discussed and validated against independent datasets such as ground-based HCHO or VOC concentration data and flux measurements.***

AR: We sincerely thank the reviewer for carefully reading our manuscript and raising this important point. Unfortunately, for China in 2020 we were unable to identify suitable independent HCHO datasets (e.g., aircraft campaigns, FTIR, or ground-based observations) for direct validation, which we acknowledge as a limitation.

Assimilation of OMPS retrievals leads to posterior results that exhibit clear improvements when compared with TROPOMI observations, as demonstrated by higher correlation coefficients (R^2) and reduced errors (MAE and RMSE) relative to the prior simulation.

To further address this limitation, we refined our methodology and emphasized a consistency analysis of the posterior results obtained by independently assimilating OMPS and TROPOMI datasets with the same framework. Here, consistency refers to cases where both assimilations indicate the same correction direction relative to the prior (i.e., both increases or both decreases). In these consistent regions, we observed significant improvements in surface ozone simulations: 81.25% of the regions showed improvements, with the mean RMSE of MDA8 ozone reduced by 24.7%. These results demonstrate that when two independent assimilations based on different satellite datasets yield similar posterior corrections in direction, ozone simulations are substantially improved, thereby supporting the robustness of our inversion. We hope the reviewer will re-evaluate the revised manuscript in light of these methodological updates and the strengthened validation through ozone.

Text in manuscript

3.3 Formaldehyde ~~total~~ columns evaluation

...

The prior and OMPS-driven posterior simulations of formaldehyde tropospheric columns were compared with the TROPOMI formaldehyde tropospheric columns to evaluate the changes in ~~Inner Mongolia, Tibet, and the northwest were minimal. This is because the assigned background uncertainty, which is proportional to~~ formaldehyde. Scatter plots together with statistical metrics (R^2, R, MAE, and

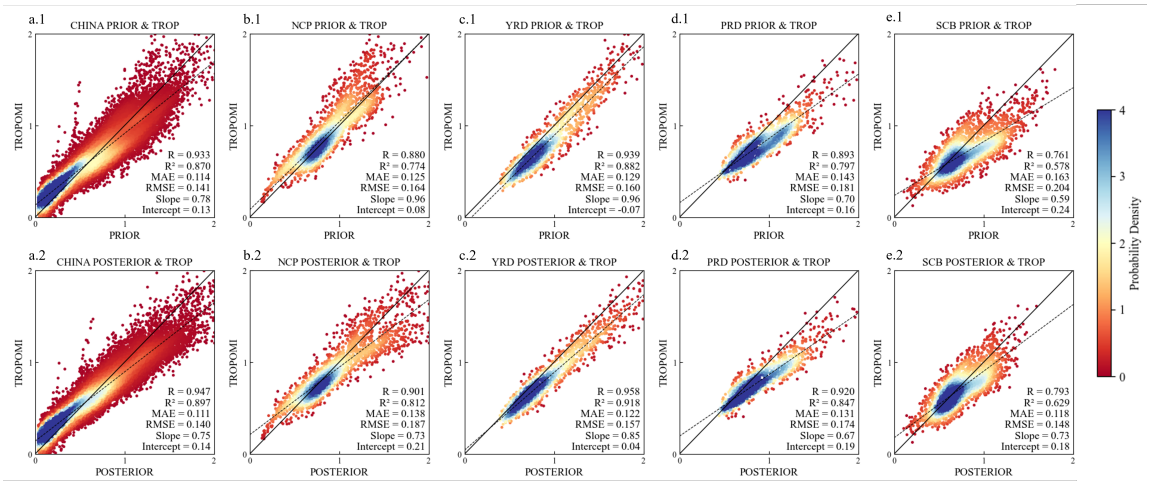

Figure 7. Scatter density plots comparing GEOS-Chem simulated formaldehyde columns with TROPOMI observations in 2020. Panels (a.1-e.1) show comparisons between prior simulations and TROPOMI, while panels (a.2-e.2) show comparisons between posterior simulations constrained by assimilating OMPS observations and TROPOMI. The regions considered are China (a), the North China Plain (b), the Yangtze River Delta (c), the Pearl River Delta (d), and the Sichuan Basin (e). The probability density of the data points is indicated by the color scale. The correlation coefficient (R), coefficient of determination (R^2), mean absolute error (MAE), root mean square error (RMSE), regression slope, and intercept are reported in each panel.

RMSE) for the ~~prior emission intensity in these regions, was particularly low, leaving limited flexibility for adjustments in the assimilation. This can be best seen in Figure 2, these areas are depicted in gray on the map, with annual total emissions below $5 \times 10^{-4} kg/m^2$, and the actual values for some grid points in these regions are even less than~~ whole country and four subregions in 2020 are presented in Figure 7. The prior simulation already shows reasonably good performance (a.1-e.1), with most points distributed close to the 1 $\times 10^{-4} kg/m^2$. ~~Though assimilating OMPS observations~~:1 line and exhibiting strong correlations with observations. Nevertheless, further improvements are still possible. After assimilating OMPS data, the posterior ~~simulation in these regionsstill remains low, resulting in little change. As illustrated in Figure 7 (a.2, a.3)~~results compared with TROPOMI show higher R^2 values across all regions, ~~the minimal changes in these areas also affected the national observation-minus-simulation discrepancies (root mean square error , RMSE), which decreased from 0.49 $\times 10^{16}$ molec/cm^2~~ indicating strengthened correlations. For China and NCP, the improvements are comparable, with R^2 increasing by about 0.027 (from 0.870 to ~~0.46 $\times 10^{16}$ molec/cm^2. However, as shown in Figure 7 (b.2) -(b.3) , when focused on the NCP region, the RMSE decreased from 0.53 $\times 10^{16}$ molec/cm^2~~ 0.897 for China, and from 0.774 to ~~0.37 $\times 10^{16}$ molec/cm^{2}effectively. As indicated in the time series plot in Figure 7 (a.1), due to the minimal changes in formaldehyde columns in Inner Mongolia, Tibet,~~ 0.812 for NCP). In the YRD, the improvement is more pronounced, with R^2 rising from 0.882 to 0.918, and the scatter around the regression line substantially reduced, with many outliers corrected. The most significant improvements occur in PRD and SCB, where R^2 increases by approximately 0.05. In these regions, the overestimations present in the prior simulations are effectively mitigated, particularly for high-value cases. In terms of RMSE and MAE, decreases

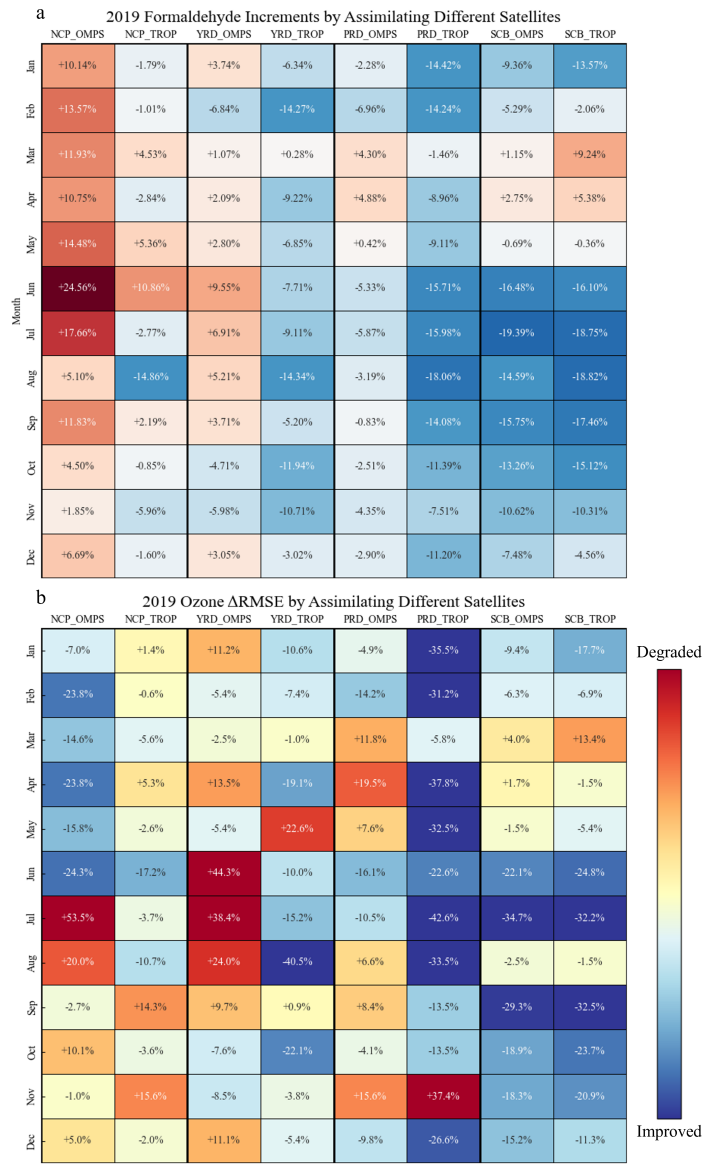

Figure 8. Monthly increments in (a) formaldehyde column concentrations between posterior and prior simulations and (b) the relative changes in MDA8 ozone RMSE (ΔRMSE) after assimilating OMPS and TROPOMI observations in 2019. Results are shown for the North China Plain, Yangtze River Delta, Pearl River Delta, and Sichuan Basin. Positive values indicate an increase relative to the prior, while negative values indicate a decrease.

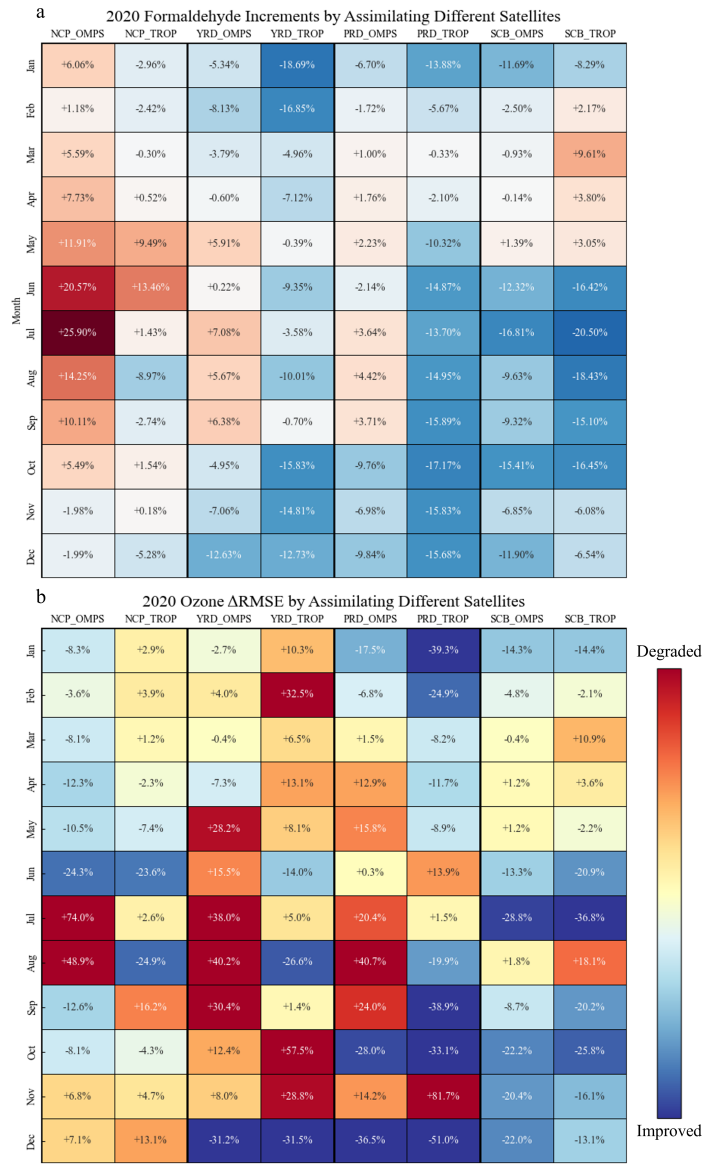

Figure 9. Monthly increments in (a) formaldehyde columns between posterior and prior simulations and (b) the relative changes in MDA8 ozone RMSE (ΔRMSE) after assimilating OMPS and TROPOMI observations in 2020. Results are shown for the North China Plain, Yangtze River Delta, Pearl River Delta, and Sichuan Basin. Positive values indicate an increase relative to the prior, while negative values indicate a decrease.

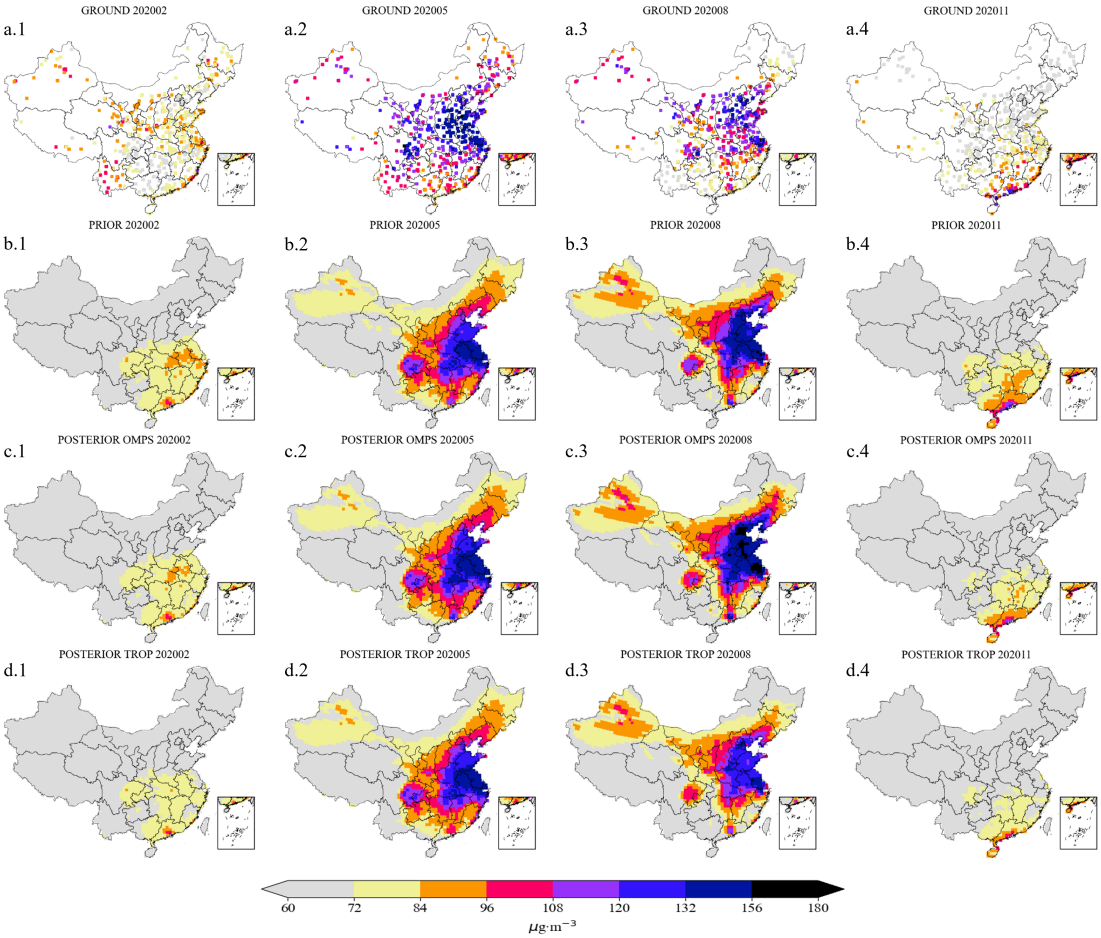

Figure 10. Spatial distributions of surface ozone concentrations in February, May, August, and November 2020. Panels (a.1-a.4) show ground-based observations, panels (b.1-b.4) show prior simulations, panels (c.1-c.4) show posterior simulations constrained by assimilating OMPS formaldehyde observations, and panels (d.1-d.4) show posterior simulations constrained by assimilating TROPOMI formaldehyde observations.

are observed in all regions except NCP. A comparison between Figures (b.1) and (b.2) indicates improvements in the low- and ~~the northwest, the nationwide monthly average formaldehyde concentrations in the posterior results are still not high enough compared to TROPOMI data. However, when we plot the time series for the NCP region alone, the results are better. The~~ mid-value ranges, whereas substantial overestimations appear in the high-value range. This issue is likely related to the instrumental errors of OMPS observations, as discussed in Sections 2.3.1 and 3.2, which introduce considerable uncertainties.

...

3.4 Impact of formaldehyde assimilation on ozone surface concentration

~~The spatial distribution prior and posterior MDA8 surface O_3 concentration simulation, as well as the corresponding observations, are plotted in Figure 8. When comparing the prior MDA8 O_3 surface concentration results with data from 1602 stations nationwide, the prior results generally capture the main hot spots of~~ The spatial distributions of observed MDA8 ~~O_3 surface concentrations, especially in July, where they closely match the ground observations. However, in the other three months shown here, the performance is not as accurate as in July.~~

~~Figure 9 illustrates the evaluation of O_3 simulation in terms of different metrics, including probability density (a), scatter plots (b), and correlation coefficients (c)~~ozone at ground stations (a.1-a.4), together with the prior (b.1-b.4) and posterior simulations based on OMPS and TROPOMI assimilation (c.1-c.4, d.1-d.4), are shown in Figure 10. As shown in ~~Figure 9 (a), the frequency distribution histogram clearly demonstrates~~ panels (b.1-b.4), pronounced ozone hotspots are observed in NCP (February, May, and August), YRD (May and August), PRD (May, August, and November), and SCB (May and August). This is very similar to the observations shown in panels (a.1-a.4). It indicates that the prior ~~ground-level O_3 simulations systematically underestimate the observed values, whereas the posterior results effectively reduce this bias. This indicates that both the overall and regional simulations of surface O_3 concentrations have been significantly improved, especially in~~ simulation captures the general patterns of ozone hotspots reasonably well, but notable biases remain. For example, ozone is clearly overestimated in PRD during February, May, and August, while underestimated in SCB during May and August. After assimilation with OMPS or TROPOMI, the ~~NCP region. As can be seen in Figure 9~~ posterior MDA8 ozone simulations retain the overall hotspot distribution, but the direction and magnitude of changes vary by region. For instance, in August, ozone concentrations increase in NCP and PRD with OMPS assimilation but decrease with TROPOMI assimilation. In February, both assimilation results decrease in YRD, although the decrease is more pronounced in the TROPOMI-based results. Moreover, many regional changes are difficult to discern visually from the spatial maps alone, highlighting the necessity of using statistical metrics to quantitatively assess ozone variations.

The RMSE values between the simulated MDA8 ozone and the ground-based observations are calculated. To better visualize the assimilation benefits, the RMSE variation either assimilating the TROPOMI or assimilating the OMPS in the four key regions are also shown in Figure 9 (b). Larger decreases in RMSE (darker blue) indicate more significant improvements, with the posterior ozone being closer to ground-based observations; conversely, larger increases in RMSE (darker red) indicate degraded performance, with the posterior ozone diverging further from the observations. In those inconsistent cases where the OMPS and TROPOMI posterior increments exhibit opposite signs (i.e., one increases while the other decreases), ozone simulation improvement is not guaranteed. For instance, in NCP

during January-April and July, in YRD during June and September, and in PRD during April, May, August, and September, one assimilation leads to improvement while the other indicates deterioration. Moreover, in several additional months both posteriors even show degradation, making it difficult to effectively evaluate the improvement in posterior ozone simulations. By contrast, ozone simulation improvements are clearly observed in consistent cases where the OMPS- and TROPOMI-constrained posteriors exhibit the same sign (i.e., both reductions in ΔRMSE). In NCP, ~~the RMSE (root mean square error) between the observed and simulated values decreasesfrom 24.44 μg/m^3 to 22.79 μg/m^3 for China and from 28.0 μg~~substantial improvements are observed in May and June, with the largest RMSE decrease in June, in agreement with the high-consistency pattern shown in Figure 9 (a). In YRD and PRD, RMSE decreases by more than 30% in December, representing the most significant improvement; in addition, PRD also shows clear improvements in January and October. These improvement months all correspond to periods of high consistency. In SCB, RMSE also decreases markedly during high-consistency months, including January, June, July, and September-December.

To further quantify ozone simulation improvements in consistent regions, statistics were performed for the months classified as consistent. Considering the similarity in monthly behavior between YRD and PRD, the two regions were combined in the analysis. The results indicate that the consistent regions include NCP in May-June, YRD/~~m^3 to 20.22 μg~~PRD in January-March and October-December, and SCB in January and June-December. Within these regions, except for March and November in YRD/~~m^3 for the NCP region. As shown in Figure 9 (c), the correlation coefficients calculated based on the monthly average time series in the NCP region show a slight improvement, while the increase is more noticeable in the southern and northeastern regions. Spatial distributions of the MDA8 surface O_3 concentrations from GEOS-Chem model-simulated prior (a) and posterior (b) results, and from ground O_3 monitoring sites (c) in January (a.1)-(c.1), April (a.2)-(c.2), July (a.3)-(c.3), October 2020 (a.4)-(c.4). Frequency histogram of the difference between the ground monitoring observed and simulated O_3 surface concentrations over China and North China Plain in 2020 (a.1, a.2) and scatter plot of the observed vs. simulated O_3 surface concentrations using either prior data (b.1, b.3) or posterior data (b.2, b.4). The correlation coefficients calculated based on prior monthly averaged time series in 2020 (c.1), and the difference between posterior and prior correlation coefficients (c.2).~~ PRD and August in SCB, all other months show ozone simulation improvements. Overall, 13 out of the 16 consistent months exhibit improvements, accounting for 81.25%, with an average RMSE reduction of 24.7%. This result suggests that constraining NMVOC emissions through formaldehyde assimilation not only substantially improves formaldehyde simulations, but also exerts a positive impact on ozone simulations, with particularly significant improvements in regions and months characterized by high consistency.

References

Boersma, K., Eskes, H., and Brinksma, E.: Error analysis for tropospheric NO2 retrieval from space, Journal of Geophysical Research: Atmospheres, 109, 2004.

Cao, H., Fu, T.-M., Zhang, L., Henze, D. K., Miller, C. C., Lerot, C., Abad, G. G., De Smedt, I., Zhang, Q., van Roozendael, M., et al.: Adjoint inversion of Chinese non-methane volatile organic compound emissions using space-based observations of formaldehyde and glyoxal, Atmospheric Chemistry and Physics, 18, 15 017–15 046, 2018.

Chance, K.: OMI/Aura Formaldehyde (HCHO) Total Column Daily L2 Global Gridded 0.25 degree x 0.25

degree V3, Greenbelt, MD, USA, Goddard Earth Sciences Data and Information Services Center (GES DISC), , accessed: [Data Access Date], 2014.

Choi, J., Henze, D. K., Cao, H., Nowlan, C. R., González Abad, G., Kwon, H.-A., Lee, H.-M., Oak, Y. J., Park, R. J., Bates, K. H., et al.: An inversion framework for optimizing non-methane VOC emissions using remote sensing and airborne observations in Northeast Asia during the KORUS-AQ field campaign, Journal of Geophysical Research: Atmospheres, 127, e2021JD035 844, 2022.

Clarisse, L., Franco, B., Van Damme, M., Di Gioacchino, T., Hadji-Lazaro, J., Whitburn, S., Noppen, L., Hurtmans, D., Clerbaux, C., and Coheur, P.: The IASI NH 3 version 4 product: averaging kernels and improved consistency, Atmospheric Measurement Techniques Discussions, 2023, 1–31, 2023.

Cooper, M. J., Martin, R. V., Henze, D. K., and Jones, D.: Effects of a priori profile shape assumptions on comparisons between satellite NO 2 columns and model simulations, Atmospheric Chemistry and Physics, 20, 7231–7241, 2020.

Duncan, B. N., Yoshida, Y., Olson, J. R., Sillman, S., Martin, R. V., Lamsal, L., Hu, Y., Pickering, K. E., Retscher, C., Allen, D. J., et al.: Application of OMI observations to a space-based indicator of NOx and VOC controls on surface ozone formation, Atmospheric Environment, 44, 2213–2223, 2010.

González Abad, G., Vasilkov, A., Seftor, C., Liu, X., and Chance, K.: Smithsonian astrophysical observatory ozone mapping and profiler suite (SAO OMPS) formaldehyde retrieval, Atmospheric Measurement Techniques, 9, 2797–2812, 2016.

Jin, J., Segers, A., Lin, H. X., Henzing, B., Wang, X., Heemink, A., and Liao, H.: Position correction in dust storm forecasting using LOTOS-EUROS v2.1: grid-distorted data assimilation v1.0, Geoscientific Model Development, 14, 5607–5622, , URL https://gmd.copernicus.org/articles/14/5607/2021/, 2021.

Jin, J., Fang, L., Li, B., Liao, H., Wang, Y., Han, W., Li, K., Pang, M., Wu, X., and Lin, H. X.: 4DEnVar-based inversion system for ammonia emission estimation in China through assimilating IASI ammonia retrievals, Environmental Research Letters, 18, 034 005, 2023.

Jung, J., Choi, Y., Mousavinezhad, S., Kang, D., Park, J., Pouyaei, A., Ghahremanloo, M., Momeni, M., and Kim, H.: Changes in the ozone chemical regime over the contiguous United States inferred by the inversion of NOx and VOC emissions using satellite observation, Atmospheric research, 270, 106 076, 2022.

Kaiser, J., Jacob, D. J., Zhu, L., Travis, K. R., Fisher, J. A., González Abad, G., Zhang, L., Zhang, X., Fried, A., Crounse, J. D., et al.: High-resolution inversion of OMI formaldehyde columns to quantify isoprene emission on ecosystem-relevant scales: application to the southeast US, Atmospheric Chemistry and Physics, 18, 5483–5497, 2018.

Lee, J.-S.: Digital image enhancement and noise filtering by use of local statistics, IEEE transactions on pattern analysis and machine intelligence, pp. 165–168, 1980.

Liu, C., Xiao, Q., and Wang, B.: An ensemble-based four-dimensional variational data assimilation scheme. Part I: Technical formulation and preliminary test, Monthly Weather Review, 136, 3363–3373, 2008.

Miyazaki, K., Bowman, K. W., Yumimoto, K., Walker, T., and Sudo, K.: Evaluation of a multi-model, multi-constituent assimilation framework for tropospheric chemical reanalysis, Atmospheric Chemistry and Physics, 20, 931–967, 2020.

Nowlan, C. R., González Abad, G., Kwon, H.-A., Ayazpour, Z., Chan Miller, C., Chance, K., Chong, H., Liu, X., O'Sullivan, E., Wang, H., et al.: Global formaldehyde products from the Ozone Mapping and Profiler Suite (OMPS) nadir mappers on Suomi NPP and NOAA-20, Earth and Space Science, 10, e2022EA002 643, 2023.

Palmer, P. I., Jacob, D. J., Chance, K., Martin, R. V., Spurr, R. J., Kurosu, T. P., Bey, I., Yantosca, R., Fiore, A., and Li, Q.: Air mass factor formulation for spectroscopic measurements from satellites: Application to formaldehyde retrievals from the Global Ozone Monitoring Experiment, Journal of Geophysical Research: Atmospheres, 106, 14 539–14 550, 2001.

Souri, A. H., Choi, Y., Jeon, W., Woo, J.-H., Zhang, Q., and Kurokawa, J.-i.: Remote sensing evidence of decadal changes in major tropospheric ozone precursors over East Asia, Journal of Geophysical Research: Atmospheres, 122, 2474–2492, 2017.

Souri, A. H., Nowlan, C. R., González Abad, G., Zhu, L., Blake, D. R., Fried, A., Weinheimer, A. J., Wisthaler, A., Woo, J.-H., Zhang, Q., et al.: An inversion of NO x and non-methane volatile organic compound (NMVOC) emissions using satellite observations during the KORUS-AQ campaign and implications for surface ozone over East Asia, Atmospheric Chemistry and Physics, 20, 9837–9854, 2020.

Xia, J., Zhou, Y., Fang, L., Qi, Y., Li, D., Liao, H., and Jin, J.: South Asia ammonia emission inversion through assimilating IASI observations, EGUsphere, 2025, 1–22, 2025.

Xue, R., Wang, S., Li, D., Zou, Z., Chan, K. L., Valks, P., Saiz-Lopez, A., and Zhou, B.: Spatio-temporal variations in NO2 and SO2 over Shanghai and Chongming Eco-Island measured by Ozone Monitoring Instrument (OMI) during 2008–2017, Journal of Cleaner Production, 258, 120 563, 2020.

Zhang, C., Liu, C., Hu, Q., Cai, Z., Su, W., Xia, C., Zhu, Y., Wang, S., and Liu, J.: Satellite UV-Vis spectroscopy: implications for air quality trends and their driving forces in China during 2005–2017, Light: Science & Applications, 8, 100, 2019.

Zhu, L., Jacob, D. J., Kim, P. S., Fisher, J. A., Yu, K., Travis, K. R., Mickley, L. J., Yantosca, R. M., Sulprizio, M. P., De Smedt, I., et al.: Observing atmospheric formaldehyde (HCHO) from space: validation and intercomparison of six retrievals from four satellites (OMI, GOME2A, GOME2B, OMPS) with SEAC 4 RS aircraft observations over the southeast US, Atmospheric chemistry and physics, 16, 13 477–13 490, 2016.

Zhu, L., Jacob, D. J., Keutsch, F. N., Mickley, L. J., Scheffe, R., Strum, M., González Abad, G., Chance, K., Yang, K., Rappenglück, B., et al.: Formaldehyde (HCHO) as a hazardous air pollutant: Mapping surface air concentrations from satellite and inferring cancer risks in the United States, Environmental Science & Technology, 51, 5650–5657, 2017.